Robust Edge Correction

J. McElvain, Xerox Corporation, El Segundo, California, USA

Abstract

Measurements of the edge characteristics of a xerographic printer are presented. Obtained using a high resolution drum scanner, these data are analyzed with the goal of quantifying edge nonlinearities. Based on these measurements, a simple model is constructed to describe the change in printed toner density for a thin border region surrounded by two larger patches. The model is subsequently used to develop a real time correction algorithm that utilizes the edge nonlinearity measurements, using a fixed point iterative approach. These corrections are shown to be significant, and strongly dependent on the levels of the surrounding patches. Furthermore, it is shown that for larger border widths, the correction is much smaller. This behavior is physically reasonable, as the correction should approach zero as the border region becomes large.

Introduction

The art of color printer calibration has been well studied,[1-5] the applications of which can be found in several consumer products today. Most of these methods employ the Neugebauer approach, whereby a series of uniform area patches is measured to develop a set of equations to describe the reflectance of a halftone pattern on paper. This set of equations, denoted the "printer model" is then inverted to determine one or more lookup tables, used to produce the desired printer output. These lookups will generally produce smooth monotonic output for each channel, and for CMYK printers there may be an additional requirement to achieve gray balance between (CMY) and K.

In many marking systems, in particular those involving electrophotography, the ink/toner densities at halftoned edges can be quite different relative to uniform regions. For xerography, average edge tangential electric fields can have a significant effect on the density of the toner cloud, as well as its proximity to the photoreceptor.[6] Likewise at edges, field components parallel to the PR surface can give rise to toner cloud displacements, and can result in artifacts such as lead-edge and trail-edge deletions.[6] Both these factors are manifested in the form of reduced dot gain, and partial dots at edges will be either significantly reduced in size or completely eliminated. Clearly, modeling each of these edge nonlinearities from a theoretical standpoint is a formidable task, and such a model would not be amenable to applications that require real time corrections.

Edge processing algorithms such as trapping and anti-aliasing are most affected by these nonlinearities. Focusing on one separation at a time, a thin strip of an intermediate digital value (C) is placed at the position of the original intersection between two patches (A and B), as shown in Figure 1. Because of the edge marking nonlinearities, the actual printed toner densities in these regions can be strongly distorted, and can lead to objectionable artifacts. Clearly these effects will be compounded for intersections where multiple color separations are present. In the case of trapping, an intentional multi-pixel "defect" is added at color interfaces to mitigate registration errors, where the width of the trap is determined by the maximum misregistration of the marking system. Generally, the color of this defect is chosen such that it is not objectionably visible in the presence of the original two intersecting colors.[7,8] For marking processes such as xerography, the printed color of the trap region may take on an undesirable color cast in the presence of nonlinearities, thus reducing the benefit of trapping. It would therefore be desirable to apply corrections to these regions in order to produce the colors that were originally intended.

Figure 1. Schematic of a common adjacency situation where a thin strip of color C is placed at an interface between larger patches A and B.

As previously mentioned, a correction algorithm involving a complete description of the edge development/transfer physics for each separation may provide an accurate edge color correction, but would generally not be practical for applications that require real time correction. On the other hand, a truly empirical correction algorithm that does not include details of the edge behavior might be computationally efficient, but would most likely provide inadequate correction in certain regions of color space. In this work, a semi-empirical approach is chosen that utilizes measurements of the printer edge characteristics. These measurements are assumed to be collected offline, and are stored in the form of lookup tables, one for each separation, to be used at run time. The correction algorithm uses these lookups in conjunction with fixed point iteration to solve for the corrected edge values, one separation at a time. Because printer edge characteristics are directly used in the calculation, the algorithm provides a correction mechanism that is robust across the device color space.

Measurement

In order to characterize the edge nonlinearities, a PostScript test master was created for each cyan, magenta, yellow, and black separations. Each single separation master contained 84 target patches, and each patch (Figure 2) consisted of a large (1/4 inch) central uniform region (contone value A) surrounded by a larger (3/4 inch) uniform patch (contone value B). Placed at the interface between A and B was a thin border of width 0.005 inches, with a contone value C; alignment marks were also positioned to enable facile location of this border region during analysis. For the 84

patches, the contone values were ramped in 14.3% increments, with the condition that $B < C \leq A$.

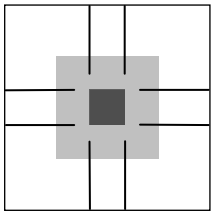

Figure 2. Schematic of a test patch used for edge characterization measurements. A large uniform patch (0.25") is surrounded by a larger patch (0.75") of a lighter color. Placed at the interface is a thin strip (0.005") with an intermediated color. The alignment marks are used to locate the interface region. Note that each patch consists of a single separation.

The four masters were then printed on a color xerographic printer, with a 600 dpi resolution, using a 170 dpi halftone. The width of the border region C was therefore equal to exactly 3 pixels in the final prints. Each of these targets was then scanned using a Crosfield 6180 drum scanner, at an approximate resolution of 8700 dpi. The resulting files were converted from RGB to CMYK (8 bits/channel) in-situ by the scanner software, resulting in uncompressed file sizes of approximately 300 MB for each patch (note that each patch contains only a single separation). A portion of one of these scans (K separation target) is shown in Figure 3, and clearly shows the detailed halftone structure. In total, 336 of theses patches were scanned.

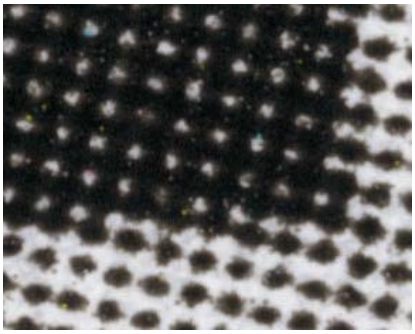

Figure 3. A portion of one patch measured with a drum scanner, for the K separation. The halftone dots are clearly visible.

Although great care was taken during the scanning to align the patches relative to the scan axes, it was still necessary to rotate and deskew the images by small amounts to compensate for image warping. Both of these operations were enabled by the placement of alignment marks on each patch, and the rotation/skew angles never exceeded 1° for all separations during post acquisition processing.

The regional scanned halftone values were converted to contone values by computing the mean digital value within a given window, where the window was assumed to include many halftone cycles. Although the scanned data values result from a convolution of the scanner modulation transfer function (MTF) with the actual printed halftones, it is a fairly good measure of the printed halftone fill factor. The mean value was measured for each of the large uniform patch regions (A or B), each of which had a known digital input value (as specified in the PostScript master). This enabled the construction of an 8 node calibration lookup table, which was interpolated using a least squares fit to a 6th order polynomial function in order to estimate the calibration for points between nodes. The calibration curve for the K separation is shown in Figure 4.

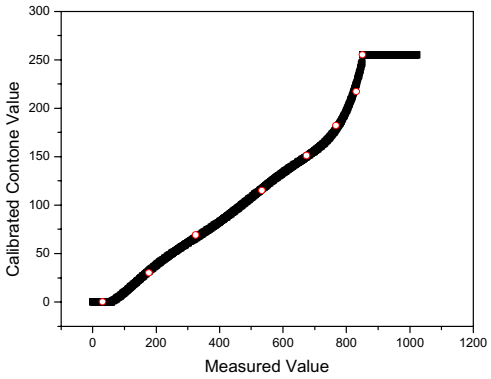

Figure 4. The calibration curve computed using a 6th order least squares polynomial fit. The circles indicate the measured values from the scanned patches.

For each patch, the behavior in the vicinity of the border region C was measured for the top, bottom, left, and right edges associated with the transitional region. This was accomplished by choosing a window with a height (width) approximately equal to the inner patch dimension (~2000 pixels @8700 dpi), and a width (height) equal to 3 pixels (@ 8700 dpi). The window was then moved from -75 to + 75 pixels relative to the center of the border region C (determined by the alignment marks), in order to measure the density profile near the transitional region. Figure 5 shows an example scan for the same patch for the top, bottom, left, and right edges for a K patch with A = 57%, B = 28%, and C = 43%. For reference, the solid line shows the theoretical response for an "ideal" halftoned border region using the measurement technique described above. As can be seen from the figure, the edge response is very similar for the four faces, suggesting minimal lead- and trail-edge deletion effects for the particular printer used.

Figure 6 compares the transition profiles for different patches with B=28%, C=43% common for all patches, and A ranging from 43% to 100%. Interestingly enough, the curves all have the same qualitative features in the vicinity of region C. At the center of C is a relatively flat "linear" region approximately 6 pixels wide, surrounded by two "nonlinear" regions that show toner densities above or below that of the central region. The 6 pixel central region is referred to as "linear", since its measured value corresponds to that which would be obtained with a large area patch; in other words, its response is linear.

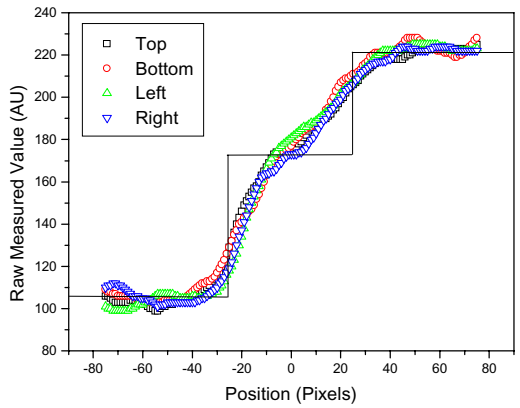

Figure 5. Example scan profiles for the top, bottom, left, and right faces of a patch. The width of the border region is approximately 43 pixels (@ 8700 dpi). For comparison, the solid line shows the ideal response in the absence of nonlinearities.

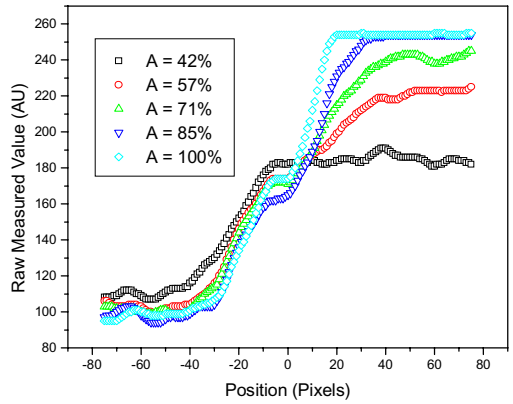

Figure 6. Plot of transition profiles for various patches with B=28% and C=42%, and ramping A values. Each of the curves has a similar qualitative shape to the left, independent of the A values.

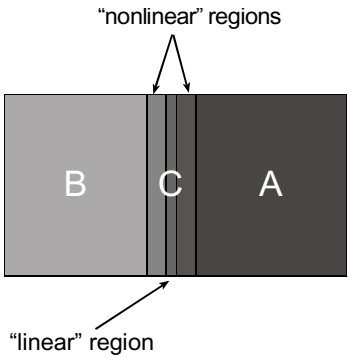

Figure 7. Illustration of subdivision of region C into a linear region sandwiched between two nonlinear regions.

Correction Model

Based on the observations regarding the qualitative profile behavior, a simple model can be constructed to describe the "average" toner density as seen by an observer for a given separation. The border region C can be subdivided into three decoupled sub-regions (Figure 7), and the average value can be described by the following expression:

$$C_\alpha^A = w_\alpha^{NL} f_\alpha\left(A_\alpha, C_\alpha^I\right) + w_\alpha^L C_\alpha^I + w_\alpha^{NL} f_\alpha\left(B_\alpha, C_\alpha^I\right) \quad (1)$$

A_α and B_α are the input values for separation α for regions A and B, respectively, and C_α^A, C_α^I are the average printed and the "intended" input levels for the border region. The coefficients w_α^L and w_α^{NL} correspond to the weights of the linear and two nonlinear regions, and are equal to the percentage of the total border region each occupies. For simplicity, it has been assumed that the weights of the two nonlinear regions are the same. The function $f_\alpha(x,y)$ describes the average measured value of the nonlinear regions, given an interface involving input levels *x* and *y*.

If the further assumption is made that the width of the nonlinear region is a constant ($t_{NL} \approx 50$ μm), the linear and nonlinear weights can be expressed in terms of the total width, T, of the border region C:

$$w_\alpha^{NL} = t_{NL}/T, \; w_\alpha^L = 1 - 2w_\alpha^{NL} \quad (2)$$

provided $0 \le w_\alpha^{NL} \le 0.5$. A constant nonlinear region width implies its contribution to the overall printed level of the border is reduced as the width of region C increases; in other words, the printed level should approach that of a uniform patch for large border widths, an intuitive result.

With knowledge of the behavior at the nonlinear regions, one can then predict the average toner density for border regions given the input contone levels and the border width. However, from the standpoint of correction the reverse problem must be solved: what is the input (or corrected) border value that will give rise to the desired border value? Equation 1 can be modified to describe this problem mathematically:

$$C_\alpha^T = w_\alpha^{NL} f_\alpha\left(A_\alpha, C_\alpha^C\right) + w_\alpha^L C_\alpha^C + w_\alpha^{NL} f_\alpha\left(B_\alpha, C_\alpha^C\right) \quad (3)$$

where C_α^T and C_α^C are the target printed value and the corrected input value, respectively.

Clearly Equation 3 cannot generally be solved by analytic means, but it can be recast into a more convenient form using Equation 2:

$$C_\alpha^C = C_\alpha^T + w_\alpha^{NL}\left[F_\alpha\left(A_\alpha, C_\alpha^C\right) + F_\alpha\left(B_\alpha, C_\alpha^C\right)\right] \quad (4)$$

where

$$F_\alpha(x,y) \equiv y - f_\alpha(x,y) \quad (5)$$

The function $F_\alpha(x,y)$ can be thought of as a measure of the departure from linearity for the "nonlinear" region of the border

area. $F_\alpha(x,y)=0$ implies the entire border region exhibits a linear response, and therefore $C_\alpha^C = C_\alpha^T$; no correction is required. Fixed point iteration can be used to solve Equation 4, with convergence guaranteed as long as the following condition is satisfied[9]:

$$w_\alpha^{NL} \partial \big/ \partial C_\alpha^C \left\{F_\alpha\left(A_\alpha, C_\alpha^C\right) + F_\alpha\left(B_\alpha, C_\alpha^C\right)\right\} < 1 \qquad (6)$$

Considering this correction model, it is therefore only necessary to measure the response of the nonlinear regions as a function of the input values present at the border (A,B,C), and use these values to compute $F_\alpha(x,y)$.

Results and Discussion

Using the collected interface data described in the Measurement section, the average values for the nonlinear region were measured for each of the patches. Prior to computing theses averages, the data values were converted using the calibration lookup tables. Each of the four sides of each patch were used to obtain an average value for the two nonlinear regions $f_\alpha(i,j)$ and $f_\alpha(k,j)$, where i and k correspond to the indices for region A and B, respectively, and j corresponds to the index for the border ($0 \le i,j,k \le 7$). Therefore, these measurements created an 8X8 table for $f_\alpha(x,y)$. For those patches that yielded duplicate measurements of a particular $f_\alpha(x,y)$, the results were averaged over the number of duplications. Figure 8 shows a 3-dimensional plot of the $f_\alpha(x,y)$ measurements for the K separation. As expected, the table is monotonic in both x and y. Furthermore, for a fixed border value C, $f_\alpha(x,y)$ increases sharply with increasing A (or B) for $A,B < C$, and saturates for values $A,B > C$. This is significant, as it implies the printed border value is more severely impacted against a lighter value (lower halftone fill factor) in comparison to a darker value.

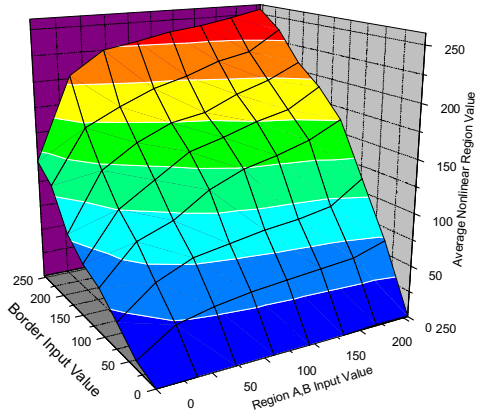

Figure 8. A 3-D plot of the measured nonlinear values for the node points chosen on the master.

The 8X8 nonlinear region tables were then interpolated to produce a 256X256 lookup table (compatible with 8 bit contone values); these were subsequently converted to "nonlinear departure" tables F[i,j], to be used for the run-time correction algorithm. A discrete version of Equation 4, invoking the fixed-point algorithm, was used to compute the corrections, shown below:

$$c[i+1] = c_t + w_{NL}\{F[a,c[i]] + F[b,c[i]]\} \qquad (7)$$

where c_t is the target printed digital value, a and b are the digital values corresponding to regions A and B, and $c[i]$ is the ith iteration of the fixed point solution to the corrected value. Iteration continues until $|c[i]-c[i-1]| < tol$. Due to the quantization errors associated with the indexing of F in Equation 7, the tolerance was set to a value of 6 to avoid oscillatory behavior. For all interface combinations tested, no more than three iterations were required, with most finding convergence in two iterations.

The algorithm was tested for border widths of 127 µm (3 pixels @600 dpi), assuming a linear width equal to 17 µm. Figure 9 shows the results of such calculations, for a variety of (A,B) combinations. Note that in all cases, the corrected border values were constrained to lie within [a,b] by the fixed point algorithm. For B=0 (Figures 9a and 9c), the corrected value is greater than the input value throughout the entire range. However, for $B \neq 0$ (Figure 9b) the correction value is actually less than the input until approximately the midpoint, after which the correction becomes greater than the input. In this case, region A creates a gain in the adjacent nonlinear region that is greater than the loss of the nonlinear region adjacent to B. For comparison, Figure 9d shows the case where A=128, B=0, with a border width of 423 µm (10 pixels @600 dpi). Clearly, the correction is relatively small in comparison to a border width of 127 µm (Figure 9a), a result that is consistent with intuition; the correction value should approach zero for large border regions.

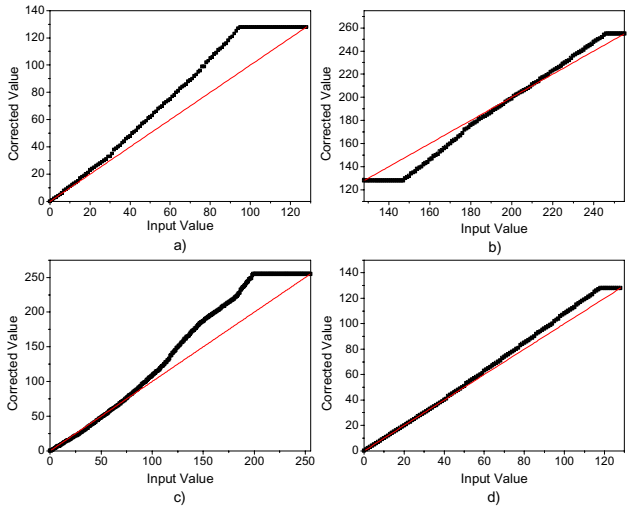

Figure 9. Corrected contone values (■) for region C as a function of input value, compared to the case of no correction (—). a) A=128, B=0, border width=127 µm; b) A=255, B=128, border width=127 µm; c) A=255, B=0, border width=127 µm; d) A=128, B=0, border width=423 µm.

This method was applied to an existing trapping algorithm for the purpose of producing a more accurate rendering of trap colors. Based on the many color pair intersections tested, the corrected

traps were far more pleasing, and showed little evidence of over-correction. Figure 10 shows a pair of micrographs for a color intersection involving (CM) against (YK), with a trap placed at the intersection. The uncorrected trap (left) shows strong evidence of pullback at the interface, resulting in a lighter than expected rendering. With the correction (right), much of the pullback is mitigated, resulting in a far less visible defect, particularly when observed from a normal viewing distance.

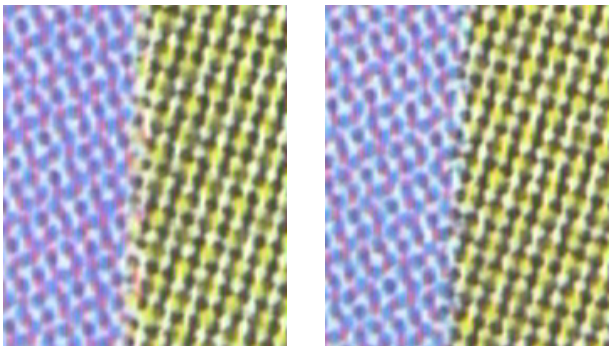

Figure 10. Micrographs of an intersection between (CM)/(MY) with a trap placed at the interface, for an uncorrected (left) and corrected (right) trap. The correction mitigates the pullback seen at the edges.

Conclusions

Edge characteristics of a xerographic printer were measured, with the goal of quantifying edge nonlinearities. A simple model was constructed to describe the change in printed toner density for a thin border region surrounded by larger patches. The model was subsequently used to develop a real time correction algorithm that utilized the edge nonlinearity measurements. For a border width of 127 μm (3 pixels @600 dpi), these corrections were shown to be significant, and strongly dependent on the levels of the surrounding patches. Furthermore, it was shown that for larger border widths, the correction was much smaller, consistent with expectations.

The simple model described here assumed a constant (and equal) width for the nonlinear regions. For halftoned edges transitioning to white, this may be inadequate, since partial dot loss in these cases may be more severe, and the "nonlinear" regions may be pushed much deeper into the edge. In these cases, it may be useful to incorporate a variable nonlinear region width (depending on the value of region B), which would result in a stronger correction. Furthermore, based on the edge characteristics of the particular printer used in these experiments, it is clear this correction model is only applicable for border regions greater than or equal to approximately 100 μm. For border widths less than this, the nonlinear regions will most likely begin to couple, creating greater error when applying this particular algorithm. Although, this correction may still be better than empirical models that do not account for the edge characteristics.

The measurements were taken using a high resolution drum scanner, which was a labor-intensive process that generated approximately 100 GB worth of image data. Clearly, this is not a practical measurement approach for systems where toner composition, xerographic setpoints, and halftone designs change on a frequent basis. Because of this, a more efficient measurement technique, analogous to uniform area calibration methods, must be developed. This presents a formidable task, since instruments with a resolution of less than 10 μm must be used for these measurements. Furthermore, alignment and rotation are also difficult to achieve to the precision required for these measurements.

Acknowledgements

This work is dedicated to the memory of Ronald E. Joiner, Jr., a teacher, mentor, and friend, who has always supported our research activities at Xerox. The author also wishes to thank S. Kim at Arc Graphics and J. Afrasiabi for help in obtaining the drum scan data.

References

1. P. Kubelka and F. Munk. Ein beitrag zur optik der farbanstriche. Z. tech Physik, 12, 593 (1931).
2. R. Rolleston, R. Bala, Accuracy of Various Types of Neugebauer Models. Proceedings of the 1st IS&T/SID Color Imaging Conference, 32 (1993).
3. P. Emmel, R.D. Hersh, Computer Graphics and Applications 19, no. 4, 54 (1999).
4. M. Zia, et al., IEEE Transactions on Image Processing 8, no. 5, 700 (1999).
5. H.E.J. Neugebauer, Die Theoretischen Grundlagen des Mehrfarbenbuchdrucks. Z. 36, 73 (1937).
6. E.M. Williams, The Physics and Technology of Xerographic Processes (Krieger, Malabar, FL 1993).
7. B.P Lawler, The Complete Guide to Trapping (Hayden, Indianapolis, IN, 1995).
8. R. Victor Klassen, Karen Braun, Robert R. Buckley, Visibility of Thin Lines on Coloured Backgrounds. Proceedings of the 6th Color Imaging Conference, 27 (1998).
9. R.L. Burden and J.D. Faires, Numerical Analysis (PWS-Kent, Boston MA, 1985).

Author Biography

Jon McElvain received a B.Sc. in Physics from the University of California at San Diego (1990), an M.A. in Physics from the University of California at Berkeley (1992), and a Ph.D. in Physics from the University of California at Santa Barbara (1996). From 1996-1999 he worked as a research scientist at UNIAX Corporation in Santa Barbara California, specializing in hybrid organic/inorganic semiconductor image processing systems. In 1999, he joined the research staff at Xerox Corporation in El Segundo, where his current interests include edge image quality and low level rendering effects.